TECNIACÚSTICA
CUENCA 2023

VIBRATION AND RADIATED NOISE COMPUTATION FROM RAILWAY SYSTEMS USING A BEM METHODOLOGY

Antonio Romero Ordóñez[1*]
Rocío Velázquez Mata[1]
Pedro Galvín Barrera[1]

[1]Universidad de Sevilla, Sevilla, España

ABSTRACT

This work studies vibration and radiated noise from railway systems using the 2.5D Boundary Element Method (BEM) formulation in the Bézier-Bernstein space. The proposed method allows the representation of the exact geometry of the track as it is done in Computer-Aided Design (CAD) models. Thus, it is possible to evaluate problems with complex geometries, which are usually not adequately represented by the standard BEM and FEM formulations. Radiated noise is computed from the normal displacement at the boundary of the rail system according to the integral representation of the sound pressure. Only the track boundary is meshed, as the radiation condition is implicitly satisfied in the BEM fundamental solution. Moreover, the methodology allows the use of arbitrary high-order elements, making it efficient for the computation of radiated noise at high frequencies. The performance of the proposed method is shown by studying the mobility and the radiated noise of an 'open' rail section.

Keywords— radiated noise, railway vibration, boundary element method, bézier curve.

1. INTRODUCTION

Rolling noise arising from railway systems is mostly due to the wheel/rail roughness. The radiated noise level depends on the train speed, rail roughness, and track mobility, among others. The track response depends on the rail, rail pads, sleepers and ballast layer. Accurate estimation of radiated noise requires a proper definition of not only track properties but also the geometry of radiating surfaces. Therefore, it is important to improve the prediction capacities of the existing numerical models in order to compute the sound radiation from the different track systems, with the aim of mitigating its effects.

This work proposes a method based on the 2.5D BEM formulation in the Bézier–Bernstein space [1] to calculate vibration and radiated noise from railway systems. This approach avoids mesh errors and enables evaluating the exact boundary geometry of complex rails sections. In addition, the representation of the field variables at nodal points instead of control variables allows an easy definition of the boundary conditions without any assumptions. The use of arbitrary high-order elements is also allowed, making it efficient for the computation of radiated noise at high frequencies.

The paper is organized as follows. First, the numerical model is presented. The 2.5D BEM formulation for elastodynamic and fluid-acoustics problems is described. The geometry and element approximations are introduced according to the Bézier–Bernstein formulation.

2. NUMERICAL MODEL

A domain Ω that comprises the track system and air medium is decomposed into different subdomains as shown in Figure 1. The subdomain decomposition corresponds to solid regions comprising the rail (Ω_{s_1}) and the rail pad (Ω_{s_2}), and the air medium (Ω_f). All of the subdomains are represented by the Boundary Element Method. Under the assumption of a longitudinally invariant problem in the z direction, the solution is obtained in the frequency-wavenumber $\omega - \kappa_z$ domain using a two-and-a-half dimensions (2.5D) formulation [1]:

$$\mathbf{a}(\mathbf{x},\omega) = \int_{-\infty}^{+\infty} \tilde{\mathbf{a}}(\tilde{\mathbf{x}},\kappa_z,\omega) e^{-\iota\kappa_z z}\, d\kappa_z \qquad (1)$$

where $\tilde{\mathbf{a}}(\tilde{\mathbf{x}},\kappa_z,\omega)$ is the frequency-wavenumber representation of a variable of interest (e.g., displacement or sound pressure), ω is the angular frequency, $\mathbf{x} = \mathbf{x}(x,y,z)$ and $\tilde{\mathbf{x}} = \mathbf{x}(x,y,0)$. The Greek letter ι denotes the unit imaginary number.

The solution of the coupled air-track system is obtained by imposing appropriate conditions at the solid-solid and

[*] ***Corresponding author***: *aro@us.es*

solid-fluid interfaces. Equilibrium of forces and compatibility of displacements must be achieved at solid interfaces; and the equilibrium of normal pressure, with null shear stress, and continuity of normal displacement are imposed at the solid-fluid interface Γ_{sf}. Each subdomain is directly coupled, and the equations are assembled into a global system.

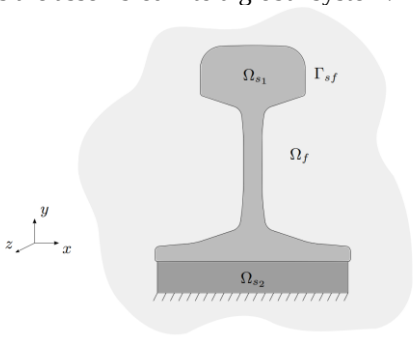

Figure 1. Boundary subdomains definition: rail (Ω_{s_1}), rail pad (Ω_{s_2}) and air medium (Ω_f).

2.1. Boundary element formulation in elastodynamics

Solids in track systems such as rail and rail pad are represented using the BEM formulation in elastodynamics. The integral representation of the displacement $\tilde{\mathbf{u}}_i$ for a point i, with zero body forces and zero initial conditions, may be written as [2]:

$$\begin{aligned}&\mathbf{c}_i(\tilde{\mathbf{x}}_i)\tilde{\mathbf{u}}_i(\tilde{\mathbf{x}}_i,\kappa_z,\omega)\\&=\int_{\Gamma_s}\Big(\tilde{\mathbf{t}}(\tilde{\mathbf{x}},\kappa_z,\omega)\tilde{\mathcal{G}}(\tilde{\mathbf{x}},\kappa_z,\omega;\tilde{\mathbf{x}}_i)\\&-\tilde{\mathbf{u}}(\tilde{\mathbf{x}},\kappa_z,\omega)\tilde{\mathcal{H}}(\tilde{\mathbf{x}},\kappa_z,\omega;\tilde{\mathbf{x}}_i)\Big)\,d\Gamma(\tilde{\mathbf{x}})\end{aligned}\tag{2}$$

where $\tilde{\mathbf{u}}(\tilde{\mathbf{x}},\kappa_z,\omega)$and $\tilde{\mathbf{t}}(\tilde{\mathbf{x}},\kappa_z,\omega)$ are displacement and traction, respectively. $\tilde{\mathcal{G}}(\tilde{\mathbf{x}},\kappa_z,\omega;\tilde{\mathbf{x}}_i)$ and $\tilde{\mathcal{H}}(\tilde{\mathbf{x}},\kappa_z,\omega;\tilde{\mathbf{x}}_i)$ are the full-space fundamental solution to displacement and traction at the point $\tilde{\mathbf{x}}$ due to a point source acting at the collocation point $\tilde{\mathbf{x}}_i$. The integral-free term $\mathbf{c}_i(\tilde{\mathbf{x}}_i)$ depends only on the boundary geometry at the collocation point $\tilde{\mathbf{x}}_i$.

The two-and-a-half-dimensional Green's function is obtained by means of the potentials $\tilde{A}_p$ and $\tilde{A}_s$ for the irrotational and equivoluminal parts of the displacement vector, respectively [3]:

$$\tilde{A}_p=\frac{\iota}{4\rho\omega^2}\left[H_0^{(2)}(\kappa_\alpha r)-H_0^{(2)}(-\iota\kappa_z r)\right]\tag{3}$$

$$\tilde{A}_s=\frac{\iota}{4\rho\omega^2}\left[H_0^{(2)}(\kappa_\beta r)-H_0^{(2)}(-\iota\kappa_z r)\right]\tag{4}$$

where $\kappa_\alpha=\sqrt{\kappa_p^2-\kappa_z^2}$ and $\kappa_\beta=\sqrt{\kappa_s^2-\kappa_z^2}$, and κ_p and κ_s represent the wavenumbers for dilatational and shear waves, respectively. $H_0^{(2)}$ is the Hankel function of the second kind. Thus, the displacement $\tilde{\mathcal{G}}_{kl}(\tilde{\mathbf{x}},\kappa_z,\omega;\tilde{\mathbf{x}}_i)$ in the k direction at $\tilde{\mathbf{x}}$ due to a point load with acting in the l direction at $\tilde{\mathbf{x}}_i$ is obtained from:

$$\tilde{\mathcal{G}}_{kl}(\tilde{\mathbf{x}},\kappa_z,\omega;\tilde{\mathbf{x}}_i)=\frac{\partial^2(\tilde{A}_p-\tilde{A}_s)}{\partial x_k\partial x_l}+\delta_{kl}\tilde{\nabla}^2\tilde{A}_s\tag{5}$$

2.2. Boundary element formulation in fluid-acoustics

The integral representation of the sound pressure in the frequency-wavenumber domain for a point $\tilde{\mathbf{x}}_i$ located at the boundary Γ_{sf} can be written as:

$$\begin{aligned}&c_i(\tilde{\mathbf{x}}_i)\tilde{p}_i(\tilde{\mathbf{x}}_i,\kappa_z,\omega)\\&=-\int_{\Gamma_{sf}}\Bigg(\iota\rho\omega\tilde{v}(\tilde{\mathbf{x}},\kappa_z,\omega)\tilde{\Psi}(\tilde{\mathbf{x}},\kappa_z,\omega;\tilde{\mathbf{x}}_i)\\&+\tilde{p}(\tilde{\mathbf{x}},\kappa_z,\omega)\frac{\partial\tilde{\Psi}(\tilde{\mathbf{x}},\kappa_z,\omega;\tilde{\mathbf{x}}_i)}{\partial\mathbf{n}}\Bigg)d\Gamma\tilde{\mathbf{x}}\end{aligned}\tag{6}$$

where $\tilde{p}(\tilde{\mathbf{x}},\kappa_z,\omega)$ and $\tilde{v}(\tilde{\mathbf{x}},\kappa_z,\omega)$ are the sound pressure and the particle normal velocity at the boundary Γ_{sf}, respectively. $\tilde{\Psi}(\tilde{\mathbf{x}},\kappa_z,\omega;\tilde{\mathbf{x}}_i)$ represents the velocity potential at point $\tilde{\mathbf{x}}$ due to a point source located at $\tilde{\mathbf{x}}_i$:

$$\tilde{\Psi}(\tilde{\mathbf{x}},\kappa_z,\omega;\tilde{\mathbf{x}}_i)=-\frac{\iota}{4}H_0^{(2)}(\kappa_f\,r)\tag{7}$$

where $\kappa_f=\sqrt{(\omega/c_f)^2-\kappa_z^2}$ is the fluid wavenumber and c_f is the sound propagation velocity.

2.3. Geometry and element approximation

The BEM formulations presented in previous sections are implemented in the Bézier-Bernstein space [1]. The Bézier-Bernstein formulation of the BEM allows for a geometry-independent field approximation. The proposed method is geometrically exact, based on Computer Aided Design (CAD), but field variables are independently approximated from the geometry. We use the Bézier–Bernstein form of a polynomial as an approximation basis to represent both geometry and field variables. The application of Bernstein polynomials for the representation of a Bézier curve $r_n(t)$ is:

$$r_n(t)=\sum_{k=0}^{n}\mathbf{b}_k B_k^n(t)\tag{8}$$

where $\mathbf{b}_k$ are the control points used to approximate the geometry and n is the curve degree. An efficient curve computation is achieved using the polar form (or blossom) of a Bézier curve $r_n(t)$, which defines a multiaffine transformation satisfying:

$$\mathbf{b}_k=\mathbf{R}(\underbrace{0,\dots,0}_{n-k},\underbrace{1,\dots,1}_{k})\tag{9}$$

where $\mathbf{R}(t_1,\dots,t_n)$ is computed as:

$$\mathbf{R}(t_1,\dots,t_n)=\sum_{\substack{I\cap J=\emptyset\\ I\cup J=\{1,2,\dots,n\}}}\prod_{i\in I}(1-t_i)\prod_{j\in J}t_j\mathbf{b}_{|J|} \tag{10}$$

Thus, a Bernstein polynomial can be formulated in polar form substituting Equation (9) into Equation (8) as follows:

$$r_n(t)=\sum_{k=0}^{n}\mathbf{R}\left(\underbrace{0,\dots,0}_{n-k},\underbrace{1,\dots,1}_{k}\right)B_k^n(t)\mathbf{R}(t,\dots,t) \tag{11}$$

The Bézier-Bernstein space is used to describe the exact element geometry as $\Gamma^j(\mathbf{x})=\mathbf{r}_n^j(t)$. Hence, the element integrals can be written on an univariate basis $t\in[0,1]$ as [1]:

$$\begin{aligned}&\int_{\Gamma^j}f(\tilde{\mathbf{x}},\kappa_z,\omega;\tilde{\mathbf{x}}_i)d\Gamma\\&=\int_0^1 f(\tilde{\mathbf{x}}(t),\kappa_z,\omega;\tilde{\mathbf{x}}_i)\left|\frac{d\mathbf{r}_n^j}{dt}\right|dt\end{aligned} \tag{12}$$

where $f(\tilde{\mathbf{x}},\kappa_z,\omega;\tilde{\mathbf{x}}_i)$ represents the integration kernel.

The BEM formulation in the Bézier-Bernstein space employs the Lagrange interpolant relative to the Bernstein basis for the field variable approximation to an element. The field approximation given by the shape function interpolates $(n+1)$ nodal values through the element shape functions ϕ^i of order n, for $i=0,\dots,n$. Then, the field approximation becomes:

$$\begin{aligned}a(t)&=\sum_{i=0}^{p}\phi^i(t)\,a^i\\&=\sum_{i=0}^{p}\left\{\sum_{k=0}^{n}c_k^iB_k^n(t)\right\}a^i\\&=\sum_{i=0}^{p}R^i(t,\dots,t)\,a^i,\end{aligned} \tag{13}$$

where the evaluation of the element shape function $\phi^i(t)$ also benefits from the computational advantages of using the polar form $R^i(t_1,\dots,t_n)$ according to Equation (10).

Once the geometry and the field approximation given by Equations (11) and (13) are introduced into the boundary integral equation of each subdomain, the integrals can be computed using a standard Gauss-Legendre quadrature with $(p+1)$ integration points whenever the collocation point is sufficiently distant from the integration element. Otherwise, the solution of singular or weakly singular integrals is numerically computed using the quadrature rule proposed in References [1, 4].

Then, Equations (2) and (6) are rewritten as follows:

$$\begin{aligned}&\tilde{\mathbf{H}}_s(\tilde{\mathbf{x}},\kappa_z,\omega;\tilde{\mathbf{x}}_i)\tilde{\mathbf{u}}(\tilde{\mathbf{x}},\kappa_z,\omega)\\&=\tilde{\mathbf{G}}_s(\tilde{\mathbf{x}},\kappa_z,\omega;\tilde{\mathbf{x}}_i)\tilde{\mathbf{t}}(\tilde{\mathbf{x}},\kappa_z,\omega)\end{aligned} \tag{14}$$

$$\begin{aligned}&\tilde{\mathbf{H}}_f(\tilde{\mathbf{x}},\kappa_z,\omega;\tilde{\mathbf{x}}_i)\tilde{p}(\tilde{\mathbf{x}},\kappa_z,\omega)\\&=\tilde{\mathbf{G}}_s(\tilde{\mathbf{x}},\kappa_z,\omega;\tilde{\mathbf{x}}_i)\tilde{v}(\tilde{\mathbf{x}},\kappa_z,\omega)\end{aligned} \tag{15}$$

where $\tilde{\mathbf{H}}_s$, $\tilde{\mathbf{G}}_s$, $\tilde{\mathbf{H}}_f$ and $\tilde{\mathbf{G}}_f$ are the fully non-symmetrical boundary element system matrices for solids and acoustic subdomains, respectively.

2.1. Subdomains coupling procedure

Solid subdomains such as rail and rail pads are coupled imposing equilibrium of forces and compatibility of displacements at solid interfaces. Equilibrium of forces at the interface is fulfilled integrating nodal tractions according to the element shape function $\mathbf{N}=[\phi_0,\dots,\phi_p]$:

$$\tilde{\mathbf{f}}=\int_{\Gamma_s}\mathbf{N}^T\tilde{\mathbf{t}}\mathbf{N}\,d\Gamma=\mathbf{T}\tilde{\mathbf{t}} \tag{16}$$

Substituting Equation (16) into Equation (14) yields the following.

$$\tilde{\mathbf{f}}=\mathbf{T}\tilde{\mathbf{G}}_s^{-1}\tilde{\mathbf{H}}_s\tilde{\mathbf{u}} \tag{17}$$

Then the coupled system for solid subdomains is obtained imposing the equilibrium and compatibility conditions at the interface:

$$\tilde{\mathbf{K}}_s(\tilde{\mathbf{x}},\kappa_z,\omega;\tilde{\mathbf{x}}_i)\tilde{\mathbf{u}}(\tilde{\mathbf{x}},\kappa_z,\omega)=\tilde{\mathbf{f}}(\tilde{\mathbf{x}},\kappa_z,\omega) \tag{18}$$

The solid and fluid subdomains are assembled next. The coupling of Equations (15) and (18) is carried out by imposition of equilibrium and compatibility conditions of normal pressure and displacement at the interface Γ_{sf} between the track system and the air medium, and null shear stresses. These conditions are fulfilled through the following system of equations [5]:

$$\begin{bmatrix}\tilde{\mathbf{K}}_s & \mathbf{R}^T\\ -\tilde{\mathbf{G}}_f\mathbf{N}^T & \tilde{\mathbf{H}}_f\end{bmatrix}\begin{bmatrix}\tilde{\mathbf{u}}\\ \tilde{p}\end{bmatrix}\begin{bmatrix}\tilde{\mathbf{f}}\\ 0\end{bmatrix} \tag{19}$$

where $\mathbf{R}$ is the coupling fluid–solid matrix which relates force and pressure at the interface Γ_{sf} :

$$\tilde{\mathbf{f}}=-\int_{\Gamma_{sf}}\mathbf{N}^T\mathbf{n}c\tilde{p}\,d\Gamma=\mathbf{R}^T\tilde{p} \tag{20}$$

where $\mathbf{n}$ is the outward normal vector at Γ_{sf}.

3. NUMERICAL EXAMPLE

In this section, the proposed method is used to study radiated noise from an open rail. A standard CEN 40E1 rail with a rail pad is considered in this example. Rail mobility and sound pressure are computed in two cases: a point load acting at i) the midpoint and ii) the edge of the rail head (see Figure 2). Displacements at the rail-pad base are constrained. The sound

pressure is obtained at a point located at a distance of 10 m horizontally and 1.5 m vertically from the center of the rail head. The problem solution is computed in the frequency range $30 - 2000$ Hz for one hundred equally spaced wavenumbers κ_z in the interval from 0 to 10 rad/m.

Three subdomains are defined to represent the rail cross section and the air medium. The material properties of the rail section are summarised in Table 1, while a fluid density $\rho_f = 1.225$ kg/m^3 and sound propagation velocity $c_f = 340$ m/s are considered for the air.

Table 1. Material properties of the rail section subdomains.

	Subdomain	
	Rail	**Rail pad**
Young's Modulus	210 [GPa]	4.8 [MPa]
Poisson's ratio	0.3	0.45
Density	7800 [kg/m^3]	10 [kg/m^3]
Damping loss factor	0.01	0.25

The boundary geometry is represented by 31 cubic Bézier patches as can be seen in Figure 2. The boundary is discretised into elements ensuring $\kappa_f h = 3$ and a nodal density per wavelength $d_\lambda = 2\pi p/\kappa_f h = 12$, where $\kappa_f = \omega/c_f$, h and p are the element length and order.

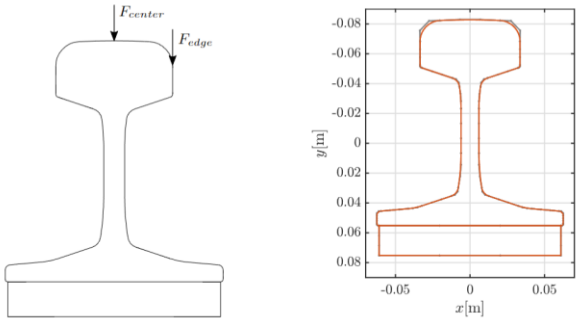

(a) (b)

Figure 2. (a) Load positions and (b) Boundary geometry of the open rail section (red line) and the related control polygons (grey line).

Figure 3.(a) shows the rail mobility at the excitation point and the sound pressure at the observation point in the air medium. Rail mobility shows a peak around 240 Hz related to the resonance of the rail mass on the rail pad in both cases. Moreover, a second peak at higher frequency appears for edge excitation due to lateral wave propagation. These results are consistent with those obtained in Reference [6]. The maximum in the sound pressure graph appears at a frequency of 450 Hz (Figure 3.(b)).

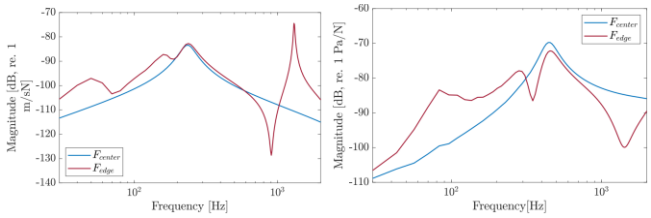

(a) (b)

Figure 3. (a) Rail mobility and (b) sound pressure.

Finally, Figure 4 shows the radiated noise near the track system due to a load acting at the midpoint of the railhead considering a frequency of 1000 Hz.

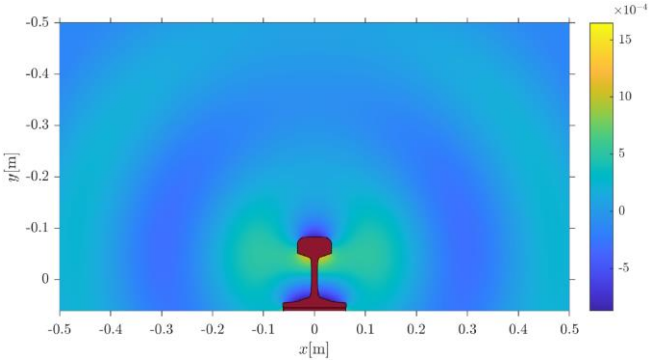

Figure 4. Radiated noise for a load acting at the midpoint of the railhead at a frequency of **1000 Hz**.

4. CONCLUSIONS

This work has proposed a 2.5D BEM formulation based on Bézier Bernstein space to study noise and vibration in railway systems. This formulation represents the exact geometry of track components that allows the analysis of complex systems commonly found on slab and urban tracks. Thus, the influence of track flexibility levels can be studied. Moreover, the proposed method is efficient for the computation of radiated noise at high frequencies since arbitrary high- order elements can be used independently of the geometry approximation. The performance of the method has been verified for an open rail section.

5. ACKNOWLEDGEMENTS

The authors would like to acknowledge the financial support provided by the Spanish Ministry of Science, Innovation and Universities under the research project PID2019-109622RB; PROYEXCEL 00659 funded by Regional Ministry of Economic Transformation, Industry, Knowledge and Universities of Andalusia; and the Andalusian Scientific Computing Centre (CICA).

6. REFERENCES

[1] A. Romero, P. Galvín, JC . Cámara-Molina JC, A. Tadeu, "On the formulation of a BEM in the Bézier–Bernstein space for the solution of Helmholtz equation". *Applied Mathematical Modelling*, vol. 74, pp. 301-319, 2019.

[2] A. Romero, A. Tadeu, P. Galvín, J. António, "2.5D coupled BEM–FEM used to model fluid and solid scattering wave". *International Journal for Numerical Methods in Engineering*, vol. 101(2), pp. 148-164, 2015.

[3] AJB. Tadeu, E. Kausel, "Green's Functions for Two-and-a-Half-Dimensional Elastodynamic Problems". *Journal of Engineering Mechanics*, vol. 126(10), pp. 1093-1097, 2000.

[4] R. Velázquez-Mata, A. Romero, J. Domínguez, A. Tadeu, P. Galvín, "A novel high-performance quadrature rule for BEM formulations". *Engineering Analysis with Boundary Elements*, vol. 140, pp. 607-617, 2022.

[5] FJ. Cruz-Muñoz, A. Romero, P. Galvín, A. Tadeu, "Acoustic waves scattered by elastic waveguides using a spectral approach with a 2.5D coupled boundary-finite element method". *Engineering Analysis with Boundary Elements*, vol. 106, pp. 47-58, 2019.

[6] CM. Nilsson, CJC Jones, DJ. Thompson, J. Ryue, "A waveguide finite element and boundary element approach to calculating the sound radiated by railway and tram rails". *Journal of Sound and Vibration*, vol. 321(3), pp. 813-836, 2009.